# Small-scale variation of snow in a regional permafrost model

**K. Gisnås[1], S. Westermann[1], T.V. Schuler[1], K. Melvold[2] and B. Etzelmüller[1]**

[1] Department of Geosciences, University of Oslo, Oslo, Norway

[2] Norwegian Water Resources and Energy Directorate, Oslo, Norway

Corresponding author: Kjersti Gisnås (kjersti.gisnas@geo.uio.no)

## Abstract

The strong winds prevalent in high altitude and arctic environments heavily redistribute the snow cover, causing a small-scale pattern of highly variable snow depths. This has profound implications for the ground thermal regime, resulting in highly variable near-surface ground temperatures on the meter scale. Asymmetric snow distributions combined with the non-linear insulating effect of snow ~~also mean that~~ the spatial average ground temperature in a 1km² area can not ~~necessarily~~ be ~~determined based on~~ the average snow cover for that area. ~~Land surface or~~ permafrost models employing a coarsely classified average snow depth will therefore not yield a realistic representation of ground temperatures. In this study we employ statistically derived snow distributions within 1km² grid cells as input to a regional permafrost model in order to represent sub-grid variability of ground temperatures. This ~~is shown to~~ improve the representation of both the average and the total range of ground temperatures. ~~The model results show that we~~ reproduce observed sub-grid ground temperature variations of up to 6°C, ~~with~~ 98% of borehole observations ~~within the~~ modelled temperature range. ~~Based on this more faithful representation of ground temperatures, we find the~~ total permafrost area of mainland Norway ~~to be nearly twice as large as what is~~ modelled without a sub-grid approach.

## 1 Introduction

High altitude and arctic environments are exposed to strong winds and drifting snow can create a small-scale pattern of highly variable snow depths. Seasonal snow cover is a crucial factor for the ground thermal regime in these areas (e.g. Goodrich, 1982; Zhang et al., 2001). This small-scale pattern of varying snow depths results in highly variable ground surface temperatures on the meter scale; up to 6 °C within areas of less than 1 km$^2$ (e.g. Gubler et al., 2011; Gisnås et al., 2014). In general, grid-based numerical land surface and permafrost models operate on scales too coarse to resolve the variability of snow depths, and are not capable of representing such small-scale variability. For the Norwegian mainland, permafrost models have been implemented with a spatial grid resolution of 1 km$^2$ (Gisnås et al., 2013; Westermann et al., 2013), and do therefore only represent the larger scale patterns of ground temperatures. As a consequence, they usually represent the lower limit of permafrost as a sharp boundary, where the average ground temperature of a grid-cell crosses the freezing temperature (0°C). In reality, the lower permafrost boundary is a fuzzy transition. Several local parameters, such as snow cover, solar radiation, vegetation, soil moisture and soil type cause a pronounced sub-grid variation of ground temperature. Different approaches have been developed to address this mismatch of scales, such as the TopoSub (Fiddes and Gruber, 2012), which accounts for the variability of a range of surface parameters using k-means clustering. At high latitudes and altitudes, one of the principal controls on the variability of ground temperature is the effect of sub-grid variation in snow cover (Langer et al., 2013; Gisnås et al., 2014). Gisnås et al. (2014) show that the observed variability in ground surface temperatures within 1 km x 1 km areas is to a large degree reproduced by only accounting for the variation in snow depths. Therefore procedures capable of resolving the small scale variability of snow depths will have the potential to considerably improve the representation of the ground thermal regime.

The spatial variation of snow is a result of several mechanisms operating on different scales in different environments (Liston et al. 2004). In tundra and alpine areas, wind-affected deposition is the dominant control on the snow distribution at distances below 1 km (Clark et al., 2011). Physically-based snow distribution models are useful over smaller areas, but are not applicable on a regional scale. The coefficient of variation (*CV*), defined as the ratio between the standard deviation and the mean, can be used as a measure of the extent of spread in a distribution. Previous studies suggest that the coefficient of variation of snow depths

($CV_{sd}$), typically ranging from low spread at 0.2 to high spread at 0.8, is well suited to reflect snow distributions in a range of environments (e.g. Liston, 2004; Winstral and Marks, 2014). Liston (2004) assigned individual values of $CV_{sd}$ to different land use classes in order to address sub-grid variability of snow in land surface schemes. According to this scheme, non-forested areas in Norway, as well as most of the permafrost areas in northern Europe ("*high-latitude alpine areas*"), would have been allocated a $CV_{sd}$ of *0.7*. A review of observed $CV_{sd}$ from a large number of snow surveys in the northern hemisphere shows a large spread of $CV_{sd}$ values, in particular within this land use class, ranging from *0.1* to *0.9* (Clark et al., 2011). This illustrates the need for improved representation of snow distribution within this land use class.

An accurate representation of the small scale snow variation highly influences the timing and magnitude of runoff in hydrological models, and a detailed picture of the sub-grid variability is of great value for the hydropower industry and in flood forecasting. Adequate representations of the snow covered fraction in land surface schemes are important for enhanced realism of simulated near surface air temperatures, ground temperatures and evaporation due to the considerable influence of snow cover on the duration of melt season and the surface albedo.

In this study we derive functional dependencies between distributions of snow depth within 1x1 km grid cells and $CV_{sd}$, based on an extensive in-situ data set from Norwegian alpine areas. In a second step, we employ the resulting snow distributions as input to the permafrost model CryoGRID1, a spatially distributed, equilibrium permafrost model (Gisnås et al., 2013). From the sub-grid representation of ground temperatures, permafrost probabilities are derived, hence enabling a more realistic, fuzzy permafrost boundary instead of a binary, sharp transition. With this approach, we aim to improve permafrost distribution modelling in inhomogeneous terrains.

## 2 Setting

The model is implemented for the Norwegian mainland, extending from 58° to 71°N. Both the topography and climate in Norway is dominated by the Scandes, the mountain range stretching south-north through Norway, separating the coastal western part with steep mountains and deep fjords from the eastern part where the mountains gradually decrease in height. The maritime climate of the west coast is dominated by low-pressure systems from the

Atlantic Ocean resulting in heavy precipitation, while the eastern parts of the Scandes have a more continental and drier climate. Mountain permafrost is present all the way to the southern parts of the Scandes, with a gradient in the lower limit of permafrost from c. 1400 to 1700 m from east to west in central southern Norway, and from c. 700 to 1200 m from east to west in northern Norway (Gisnås et al., 2013). While permafrost is also found in mires at lower elevations both in southern and northern Norway, most of the permafrost is located in exposed terrain above the tree line~~. This environment is dominated by~~ strong winds result~~ing~~ in heavy redistribution of snow.

In-situ records of snow depth data used to establish the snow distribution scheme were collected at the Hardangervidda mountain plateau in the southern part of the Scandes (Fig. 1). It is the largest mountain plateau in northern Europe, located at elevations from 1000 to above 1700 meters a.s.l., with occurrences of permafrost in the highest mountain peaks. The terrain is open and slightly undulating in the east, while in the west it is more complex with steep mountains divided by valleys and fjords. The mountain range represents a significant orographic barrier for the prevailing westerly winds from the Atlantic Ocean, giving rise to large variations in precipitation and strong winds, two agents promoting a considerably wind-affected snow distribution. Mean annual precipitation varies from 500 to more than 3000 mm over distances of a few tens of kilometres, and maximum snow depths can vary from ~~zero~~ to more than 10 meters over short distances (Melvold and Skaugen, 2013).

## 3 Model description

### 3.1 A statistical model for snow depth variation

The Winstral terrain-based approach (Winstral et al., 2002) is applied over the entire Norwegian mainland using the 10-meter national digital terrain model from the Norwegian Mapping Authority (available at Statkart.no), with wind data from the NORA10 dataset (Section 4.1) used to indicate the distribution of prevailing wind directions during accumulation season.

The terrain-based exposure parameter (*Sx*), ~~described in detail in~~ Winstral et al. (2002)~~,~~ quantifies the extent of shelter or exposure of the grid-cell ~~considered~~. *Sx* is determined by the slope between the grid-cell and the cells of greatest upward slope in the upwind terrain. The upwind terrain is defined as a sector towards the prevailing wind direction *d* constrained by

the maximum search distance (*dmax* = 100 m) and a chosen width (*A*) of 30° with the two azimuths extending 15° to each side of *d* (see Fig. 2). The cell of the maximum upward slope is identified for each search vector, separated by 5° increments. This gives in total seven search vectors for each of the eight 30° wide sectors. *Sx* for the given grid-cell is finally calculated as the average of the maximum upward slope gradient of all seven search vectors:

$$Sx_{d,A,dmax}(x_i y_i) = max\left[\tan\left(\frac{Z(x_v,y_v)-Z(x_i,y_i)}{[(x_v-x_i)^2+(y_v-y_i)^2\,]^{0.5}}\right)\right] \quad (1)$$

where *d* is the prevailing wind direction, $(x_i, y_i)$ are the coordinates of the considered grid-cell, and $(x_v, y_v)$ are the sets of all cell coordinates located along the search vector defined by ($x_i$, $y_i$), *A* and *dmax*. This gives the degree of exposure or shelter in the range -1 to 1, where negative values ~~indicate~~ exposure.

To estimate a realistic degree of exposure based on the observed wind pattern at a local site, *Sx* was computed for each of the eight prevailing wind directions *d = [0°, 45°, 90°, 135°, 180°, 225°, 270°, 315°]*, and weighted based on the wind fraction ($wf_d$). $wf_d$ accounts for the amount of different exposures in the terrain at various wind directions, and represents the fraction of hourly wind direction observations over the accumulation season for the eight wind directions. The period of wind directions influencing the redistribution of snow is ~~here chosen as~~ January to March. Wind speeds below a threshold of 7 $ms^{-1}$ are excluded, as this threshold is considered a lower limit required for wind drifting of dry snow (Li and Pomeroy, 1997; Lehning and Fierz, 2008). We assume that the snow distribution at snow maximum is highly controlled by the terrain and the general wind exposure over the winter season, and we do not account for the variation in snow properties over the season that controls how much snow is available for transport at a given time.

The calculated *Sx* parameter values are used as predictors in different regression analyses to describe the $CV_{sd}$ within 1 x 1 km derived from an Airborne Laser Scanning (ALS) of snow depths (see Sect. 4.1). The coefficient of variation of exposure degrees ($CV_{Sx}$) within each *1x1* km grid cell is computed by aggregating the *Sx* map from 10 meter to 1 km resolution according to:

$$cV_{Sx} = \mathrm{std}(e^{Sx})/\mathrm{mean}(e^{Sx}) \quad (2)$$

*Sx*-values below the 2.5$^{th}$ and above 97.5$^{th}$ percentiles of the *Sx*-distributions are excluded, giving $Sx \approx [-0.2, 0.2]$. Three regression analyses were performed to reduce the RMS between $CV_{Sx}$ and observed $CV_{sd}$, where additional predictors such as elevation above treeline (*z*) and

maximum snow depth ($\mu$) ~~successively~~ have been included (Table 1). Elevation above treeline is chosen as predictor to account for the increased wind exposure with elevation. Ideally, wind speed should be included as predictor. However, the NORA10 dataset (Section 4.1) does not sufficiently reproduce the local variations in wind speeds over land, especially not at higher elevations and for terrain with increased roughness. Because of the strong gradient in treeline and general elevation of mountain peaks from high mountains in the south to lower topography in the north of Norway, applying only elevation as predictor would result in an underestimation of redistribution in the north.

### 3.2 CryoGRID 1 with an integrated sub-grid scheme for snow variation

The equilibrium permafrost model CryoGRID 1 (Gisnås et al., 2013; Westermann et al., 2015) provides an estimate for the *MAGST* (Mean annual ground surface temperature) and *MAGT* (Mean Annual Ground Temperature at the top of the permafrost or at the bottom of the seasonal freezing layer) from freezing ($FDD_a$) and thawing ($TDD_a$) degree days in the air according to

$$MAGST = \frac{TDD_a \times nT - FDD_a \times nF}{P} \quad (3)$$

and

$$MAGT = \begin{cases} \frac{(TDD_a * nT * r_k - FDD_a * nF)}{P} & \text{for } K_t TDD_s \leq K_f FDD_s \\ \frac{\left(TDD_a * nT - \frac{1}{r_k} * FDD_a * nF\right)}{P} & \text{for } K_t TDD_s \geq K_f FDD_s \end{cases} \quad (4)$$

where $P$ is the period that $FDD_a$ and $TDD_a$ are integrated over, $r_k$ is the ratio of thermal conductivities of the ground in thawed and frozen states (assuming that heat transfer in the ground is entirely governed by heat conduction), while $nT$ and $nF$ are semi-empirical transfer-functions including a variety of processes in one single variable (see Gisnås et al., 2013; Westermann et al., 2015 for details).

The winter $nF$-factor relates the freezing degree days at the surface to the air and thus accounts for the effect of the winter snow cover, and likewise the $nT$-factor relates the thawing degree days at the surface to the air and accounts for the surface vegetation cover:

$$FDD_s = nF * FDD_a \quad \text{and} \quad TDD_s = nT * TDD_a \quad (5)$$

Variation in observed *n*-factors for forests and shrubs are relatively small, with *nT*-factors typically in the range 0.85 to 1.1, and *nF*-factors in the range 0.3 to 0.5 (Gisnås et al., 2013). ~~Following Gisnås et al. (2013) f~~orest, shrubs and mires are assigned *nT*-factors 0.9/1.0/0.85 and *nF*-factors 0.4/0.3/0.6, respectively.

Observed variations in *nT* and *nF* within the open non-vegetated areas are comparably large, with values typically in the range 0.4 – 1.2 for *nT* and 0.1 – 1.0 for *nF*. The variability is related to the high impact and high spatial variability of snow depths (Gisnås et al., 2014). While *nF* accounts for the insulation from snow due to low thermal conductivity, *nT* indirectly compensates for the shorter season of thawing degree days at the ground surface in areas with a thick snow cover. Relationships between *n*-factors for open areas and maximum snow depths are established based on air and ground temperature observations together with snow depth observations at the end of accumulation season at the 13 stations in southern Norway, presented in Hipp (2012) and at arrays of nearly 80 loggers at Finse and Juvvasshøe (Gisnås et al., 2014) (Fig. 3):

$$nF = -0.17 * \ln(\mu) + 0.25 \quad (6)$$

$$nT = -0.13 * \mu + 1.1 \quad (7)$$

The relationships between *n*-factors and snow cover in open areas are shown to be consistent within the two sites in southern Norway (Gisnås et al. 2013 and ~~Gisnås et al.~~ 2014). Due to lack of field observations including all required variables at one site in northern Norway, the relation is not tested for this area. However, it fits very well with a detailed study with 107 loggers recording the variation in ground surface temperature at a lowland site in Svalbard (Gisnås et al. 2014). Other factors, such as solar radiation and soil moisture, have minor effects on the small-scale variation in ground surface temperatures in these areas. Gisnås et al (2014) demonstrated that most of the sub-grid variation in ground temperatures within 1 km x 1 km areas in Norway and Svalbard was reproduced by including only the sub-grid variation of snow depths. In other areas other parameters than snow depth might have a larger effect on the ground surface temperatures, and should be accounted for in the derivation of *n*-factors.

We assume that the distribution of maximum snow depths within a grid cell with a given $CV_{sd}$ and average maximum snow depth ($\mu$) follows a *gamma* distribution with a probability density function (PDF) given by:

$$f(x;\ \alpha,\beta) = \frac{1}{\beta^{\alpha}\Gamma(\alpha)} x^{\alpha-1} e^{-\frac{x}{\beta}} \quad (8)$$

with a *shape* parameter $\alpha = CV_{sd}^{-2}$ and a *rate* parameter $\beta = \mu * CV_{sd}^{2}$ (e.g. Skaugen et al., 2004; Kolberg and Gottschalk, 2006). The average maximum snow depth corresponds to the coarse scale snow observation, and the original coarse scale snow depth is therefore conserved in the sub-grid snow distribution. Corresponding *n*-factors are computed for all snow depths (*x*) based on Eq. 6 and 7, and related to the PDF (Eq. 8). The model is run for each *nF* from 0 to 1 with 0.01 spacing, giving 100 model realizations. Each realization corresponds to a unique snow depth, represented with a set of *nF* and *nT* factors. Based on the 100 realizations a distribution of *MAGST* and *MAGT* are calculated for each grid cell, where the potential permafrost fraction is derived as the percentage of sub-zero *MAGT*. A schematic overview of the model chain and the evaluation is shown in Fig. 4. To assess the sensitivity of the choice of the theoretical distribution function, the model was also run with PDFs following a *lognormal* distribution, given by (e.g. Liston, 2004):

$$f(x;\lambda,\zeta) = \frac{1}{x\zeta\sqrt{2}} e^{\left\{-\frac{1}{2}\left[\frac{\ln(x)-\lambda}{\zeta}\right]^2\right\}} \quad (9)$$

where

$$\lambda = \ln(\mu) - \frac{1}{2}\zeta^2, \quad \zeta^2 = \ln(1 + CV_{sd}) \quad (10)$$

### 3.3 Model evaluation

The $CV_{sd}$ was derived for 0.5 km x 1 km areas based on the ALS snow depth data (Section 4.1) resampled to 10 x 10 meter resolution. Each 0.5 x 1 km area includes 500 to 5000 grid cells 10 x 10 m, depending on the area masked out due to lakes or measurement errors. There were > 4000 grid cells in 70% of the areas. Goodness of fit evaluations for the theoretical *lognormal* and *gamma* distributions applying the Anderson-Darling test in MATLB [adtest.m (Stephens, 1974)] were conducted for each distribution. Parameters for gamma (*shape* and *rate*) and lognormal (*mu*, *sigma*) distributions were estimated by maximum likelihood as implemented in the MATLAB functions gamfit.m and lognfit.m.

The results of the permafrost model are evaluated with respect to the average *MAGST* and *MAGT* within each grid cell, as well as the fraction of sub-zero *MAGST*. For the evaluation runs the model is forced with climatic data for the hydrological year corresponding to the observations. The performance in representing fractional permafrost distribution is evaluated

at two field sites where arrays of 26 (Juvvasshøe) and 41 (Finse) data loggers have measured the distribution of ground surface temperatures at 2 cm depth within 500 x 500 meter areas for the hydrological year 2013 (Gisnås et al., 2014). The general lower limits of permafrost are compared to permafrost probabilities derived from BTS (basal temperature of snow) - surveys (Haeberli, 1973; Lewkowicz and Ednie, 2004), conducted at Juvvasshøe and Dovrefjell (Isaksen et al., 2002). The model performance of *MAGST* is evaluated with data from 128 temperature data loggers located a few cm below the ground surface in the period 1999 - 2009 (Farbrot et al., 2008; Isaksen et al., 2008; Ødegaard et al., 2008; Farbrot et al., 2011; Isaksen et al., 2011; Farbrot et al., 2013). The loggers represent all vegetation classes used in the model, and spatially large parts of Norway (Fig. 2). Four years of data from 25 boreholes (Isaksen et al., 2007; Farbrot et al., 2011; Isaksen et al., 2011; Farbrot et al., 2013) are used to evaluate modelled *MAGT* (Fig. 1). Tables of ground surface temperature loggers (Table S1) and boreholes used for validation (Table S2) are included in the supplementary material.

# 4 Data

## 4.1 Forcing and evaluation of the snow distribution scheme

Wind speeds and directions during the snow accumulation season are calculated from the boundary layer wind speed and direction at 10 meter above surface in the Norwegian Reanalysis Archive (NORA10) wind dataset. NORA10 is a dynamically downscaled dataset of ERA -40 to a spatial resolution of 10-11 km, with hourly resolution of wind speed and direction (Reistad et al., 2011). The dataset is originally produced for wind fields over sea, and underestimates the wind speeds at higher elevation over land (Haakenstad et al., 2012). Comparison with weather station data revealed that wind speeds above the tree line are underestimated by about 60% (Haakenstad et al., 2012). For these areas the forcing dataset has been scaled linearly increased by 60 %.

The snow distribution scheme is derived from an ALS snow depth over the Hardangervidda mountain plateau in southern Norway (Melvold and Skaugen, 2013). The ALS survey is made along six transects, each covering a 0.5 x 80 km area with nominal 1.5 x 1.5 m ground point spacing. The survey was first conducted between 3rd and 21st of April 2008, and repeated in the period 21st-24th April 2009. The snow cover was at a maximum during both surveys. A baseline scan was performed 21st of September 2008 to obtain the elevation at minimum snow

cover. The ALS data are presented in detail in Melvold and Skaugen (2013). Distributions of snow depth, represented as $CV_{sd}$, are calculated for each 0.5 x 1 km area, based on the snow depth data resampled to 10 x 10 meter resolution. About 400 cells of 0.5 x 1 km exist for each year, after lakes and areas below treeline are excluded.

The snow distribution scheme is validated with snow depth data obtained by ground penetrating radar (GPR) at Finse (60°34'N, 7°32'E, 1250-1332 m a.s.l.) and Juvvasshøe (61°41'N, 8°23'E, 1374-1497 m a.s.l.). The two field sites are both located in open, non-vegetated alpine landscapes with major wind re-distribution of snow. ~~However,~~ they differ with respect to mean maximum snow depth (~2 m / ~1 m), average winter wind speeds (7-8/10-14 m/s) and topography (very rugged at Finse, while steep, but less rugged at Juvvasshøe). ~~The timing of the~~ snow surveys were late March to April (2009, 2012-2014) around maximum snow depth, but when the snow pack was still dry. The GPR surveys at Finse are constrained to an area of 1x1 km, while at Juvvasshøe they cover several square kilometres, but with lower observation density. The GPR data from the end of the accumulation season in 2013 are presented in Gisnås et al. (2014), and the data series from the other years are obtained and processed following the same procedures, described in detail in Dunse et al. (2009). The propagation speed of the radar signal in dry snow was derived from the permittivity and the speed of light in vacuum, with the permittivity obtained from snow density using an empirical relation (Kovacs et al., 1995). The snow depths were determined from the two-way travel time of the reflection from the ground surface and the wave-speed. Observations were averaged over 10 x 10 meter grid cells, where grid cells containing less than three samples were excluded. The $CV_{sd}$ for 1x1 km areas are computed based on the 10-meter resolution data.

## 4.2 Permafrost model setup

The climatic forcing of the permafrost model is daily gridded air temperature and snow depth data, called the *seNorge* dataset, provided by the Norwegian Meteorological Institute and the Norwegian Water and Energy Directorate. The dataset, available for the period 1961 – 2015, is based on air temperature and precipitation data collected at the official meteorological stations in Norway, interpolated to 1 x 1 km resolution applying Optimal Interpolation as described in Lussana et al. (2010). Snow depths are derived from the air temperature and precipitation data, using a snow algorithm accounting for snow accumulation and melt,

temperature during snow fall and compaction (Engeset et al., 2004; Saloranta, 2012). Freezing- ($FDD_a$) and thawing ($TDD_a$) degree days in the air are calculated as annual accumulated negative (*FDD*) and positive (*TDD*) daily mean air temperatures, and maximum annual snow depths ($\mu$) are derived directly from the daily gridded snow depth data. The CryoGRID 1 model is implemented at 1 x 1 km resolution over the same grid as the *seNorge* dataset.

Soil properties and surface cover is kept as in Gisnås et al. (2013), with five land cover classes; *forest*, *shrubs*, *open non-vegetated areas*, *mires* and *no data*, based on CLC level 2 in the Norwegian Corine Land Cover map 2012 (Aune-Lundberg and Strand, 2010). Sub-grid distributions of snow are only implemented for *open non-vegetated areas*.

# 5 Results

## 5.1 Observed snow distributions in mountain areas of Norway

$CV_{sd}$ within 1 x 1 km areas in the ALS snow survey at Hardangervidda ranged from 0.15 to 1.14, with mean and median of respectively 0.58 and 0.59. According to the Anderson-Darling goodness of fit evaluations 70 out of 932 areas had a snow distribution within the 5% significance interval of a *gamma* distribution, while only 1 area was within the 5% significance interval of a *lognormal* distribution. Although the null hypothesis rejected more than 90% of the sample distributions, the *Anderson-Darling Test Score* was all over lower for the *gamma* distribution, indicating that the observed snow distributions are closer to a *gamma* than to a *lognormal* theoretical distribution (Fig. 5). For lower lying areas with less varying topography and shallower snow depths, in particular in the eastern parts of Hardangervidda, the observed snow distributions were similarly close to ~~a *lognormal* as to a *gamma*~~ distribution. In higher elevated parts with more snow to the west of the plateau the snow distributions were much closer to a *gamma* distribution. Based on these findings a *gamma* distribution was used in the main model runs, while a model run with *lognormal* distributions of snow was made to evaluate the sensitivity towards the choice of the distribution function (Section 3.2).

## 5.2 Evaluation of the snow distribution scheme

Three regression models for $CV_{sd}$ as a function of the terrain-based parameter *Sx*, elevation (*z*) and mean maximum snow depth ($\mu$) were calibrated with the snow distribution data from the ALS snow survey over the Hardangervidda mountain plateau (Table 1). *Model 1* results in a root mean square error (*RMSE*) of only *0.14*, however, the correlations of the distributions are significantly improved by including *elevation* as predictor (*Model 2;* $R^2 = 0.52$). By including *maximum snow depth* as additional predictor (*Model 3*) the model improves slightly to $R^2$ = 0.55 (Fig. 6). The distribution of $CV_{sd}$ (example of *Model 3* in Fig. 8, left) shows increased values in areas of rougher topography (western side of Norway) and higher elevations (central part following the Scandes), with maximum $CV_{sd}$ up to 1.2 in the Lyngen Alps and at peaks around Juvvasshøe (Fig. 1, site 2 and 4). The lowest values of *0.2-0.3* are modelled in larger valleys in south eastern Norway, where elevations are lower and topography gentler.

The regression models for $CV_{sd}$ are validated with data from GPR snow surveys at Juvvasshøe and Finse (Table 1). The correlation for *Model 1* is poor, with $R^2 = 0.04$ and Nash-Sutcliff model efficiency (*ME*) = -0.7 (Table 1). *Model 2* improves the correlation significantly, while the best fit is obtained with *Model 3* (Fig. 6, *RMSE = 0.094*, $R^2 = 0.62$ and *ME = 0.61*). The improvement in *Model 3* compared to *Model 2* is more pronounced in the validation than in the fit of the regression models, and is mainly a result of better representation of the highest $CV_{sd}$-values. The validation area at Juvvasshøe is located at higher elevations than what is represented in the ALS snow survey data set and undergoes extreme redistribution by wind. The representation of extreme values therefore has a high impact in the validation run.

## 5.3 Modelled ground temperatures for mainland Norway

The main results presented in this section are based on the model run with 100 realizations per grid cell, applying *gamma* distributions over the $CV_{sd}$ from *Model 3*. The main results are given as averages over the 30-year period 1981 – 2010. According to the model run, in total 25 400 km$^2$ (7.8 %) of the Norwegian mainland is underlain by permafrost in an equilibrium situation with the climate over the 30-years period 1981-2010 (Fig. 1). 12 % of the land area features sub-zero ground temperatures in more than 10% of a 1 km grid cell, and is classified as sporadic (4.4 %), discontinuous (3.2 %) or continuous (4.3 %) permafrost (Fig. 1). In comparison, the model run without a sub-grid variation results in a permafrost area of only 13460 km$^2$, corresponding to 4.1% of the model domain (Table 2). The difference is

illustrated for Juvvasshøe (Fig. 7, a) and Dovrefjell (c), where the sub-grid model ~~very~~ well reproduces the observed lower limit of permafrost based on borehole temperatures and BTS-surveys. In contrast, the model without sub-grid variability indicates a hard line for the permafrost limit at much higher elevations (Fig. 7, b and d). At Juvvasshøe, the model without sub-grid distribution still reproduces the permafrost limit to some extent because of the large elevation gradient. At Dovrefjell, where the topography is much gentler, the difference between the models is much larger and the approach without sub-grid distribution is not capable of reproducing the observed permafrost distribution. The modelled permafrost area for model runs applying the other models for $CV_{sd}$ and theoretical distribution functions are summarized in Table 2.

The standard deviations of the modelled sub-grid distribution of MAGT range from 0 °C to 2.5 °C (Fig. 8, right). The highest *standard deviation* values are found in the Jotunheimen area, where modelled sub-grid variability of MAGT is up to 5 °C. Also at lower elevations in south eastern parts of Finnmark *standard deviations* exceed 1.5 °C. Here, the $CV_{sd}$ values are below 0.4, but because of cold ($FDD_a$ < -2450 °C) and dry (max SD < 0.5 meters) winters even small variations in the snow cover ~~result in~~ large effects on the ground temperatures.

Close to 70% of the modelled permafrost is situated within open, non-vegetated areas above treeline, classified as mountain permafrost according to Gruber and Haeberli (2009). This is the major part of the permafrost extent both in northern and southern Norway. In northern Norway, the model results indicate that the lower limit of continuous / sporadic mountain permafrost decreases eastwards from 1200/700 meters a.s.l., respectively, in the west to 500/200 meters in the east. In southern Norway, the southernmost location of continuous mountain permafrost is in the mountain massif of Gaustatoppen at 59.8°N, with continuous permafrost above 1700 meters a.s.l. and discontinuous permafrost down to 1200 m a.s.l. In more central southern Norway the continuous mountain permafrost reaches down to 1600 meters a.s.l in the western Jotunheimen and Hallingskarvet, and down to 1200 meters a.s.l. in the east at the Swedish border. The sporadic mountain permafrost extends around 200 meters further down both in the western and eastern parts.

### 5.4 Evaluation of CryoGRID 1 with sub-grid snow distribution scheme

The observed and modelled $CV_{sd}$ values at the field sites were 0.85 and 0.80 at Juvvasshøe, and 0.71 and 0.77 at Finse. At Juvvasshøe the observed fraction of loggers with *MAGST*

below 0°C was 77 %, while the model result indicates an aerial fraction of 64 %. Similarly, at Finse the observed negative *MAGST* fraction was 30 %, while the model indicates 32 %. The measured ranges of MAGST within the 1 km x 1 km areas were relatively well reproduced by the model (Table 3). The average MAGST within each field area was also improved compared to a model without a sub-grid representation of snow (Table 3, in parenthesis).

58% of the observed *MAGSTs* are captured by the modelled range of *MAGST* for the corresponding grid cell, and 87% within 1°C outside the range given by the distribution. The overall correlation between observed *MAGST* and average modelled *MAGST* for a grid cell is fairly good with *RMSE*, $R^2$ and *ME* of 1.3°C, 0.65 and 0.37, respectively (Fig. 9, left). The measured *MAGT* was within the range of modelled *MAGT* in all boreholes except ~~of~~ one, ~~this being~~ 0.2°C outside the range. All the average modelled *MAGT* are within ±1.6°C of observations, while 90 % are within 1°C. The *RMSE* between the observed and modelled average *MAGT* is 0.6°C (Fig. 9, right).

The evaluation of the model runs with all three $CV_{sd}$-models, as well as *lognormal* instead of *gamma* distribution functions are summarized in Table 2. The highest correlation between observed and mean *MAGST* and *MAGT* was obtained by *Model 3*, but *Model 2* yielded similar correlations. All three model runs capture 58 % of the observed *MAGST* and more than 98 % of the observed *MAGT* within the temperature range of the corresponding grid cell. The total area of modelled permafrost is 9% less when applying the simplest snow distribution model (*Model 1*) compared to the reference model (*Model 3*), while the same model without any sub-grid distribution results in 47 % less permafrost area. With a *lognormal* distribution the modelled permafrost area is 18 % less (*Model 3*) than with a *gamma* distribution.

# 6 Discussion

## 6.1 The effect of a statistical representation of sub-grid variability in a regional permafrost model

The total distribution of modelled permafrost with the sub-grid snow scheme corresponds to 7.8% of the Norwegian land area, while the modelled permafrost area without a sub-grid representation of snow ~~c.~~ 4%. This large difference in total modelled permafrost area stems exclusively from differences in the amount of modelled permafrost in mountains above the

treeline. In these areas the snow distribution is highly asymmetric ~~with~~ a majority of the area ~~having~~ below average snow depths. Because of the non-linearity in the insulating effect of snow cover the mean ground temperature of a grid cell is not~~, and is often~~ far from~~, the same as~~ the ground temperature below the average snow depth. Often, the majority of the area in high, wind exposed mountains is nearly bare blown with most of the snow blown into terrain hollows. Consequently, most of the area experiences significantly lower average ground temperatures than with an evenly distributed, average depth snow cover. In mountain areas with a more gentle topography and relatively small spatial temperature variations, an evenly distributed snow depth will result in large biases in modelled permafrost area, as illustrated at Dovrefjell in Fig. 7. This study ~~is~~ clear evidence that the sub-grid variability of snow depths should be ~~accounted for~~ in model approaches targeting the ground thermal regime and permafrost distribution.

The model reproduces the large range of variation in sub-grid ground temperatures, with standard deviations up to 2.5 °C~~. This is in accordance with~~ the observed small-scale variability of up to 6 °C within a single grid cell (Gubler et al., 2011; Gisnås et al., 2014). Inclusion of sub-grid variability of snow depths in model ~~approaches~~ ~~allows for~~ a more adequate representation of the gradual transition from permafrost to permafrost-free areas in alpine environments, and ~~thus~~ a better estimation of permafrost area. ~~With~~ a warming ~~of the~~ climate, a model without such a sub-grid representation would respond with an abrupt decrease in permafrost extent. In reality, bare blown areas with mean annual ground temperatures of -6 °C need a large temperature increase to thaw. Increased precipitation as snow would also warm the ground; however, bare blown areas may still be bare blown with increased snow accumulation during winter. A statistical snow distribution reproduces this effect, also with an increase in mean snow depth.

CryoGRID1 is a simple modelling scheme delivering a mean annual ground temperature at the top of the permanently frozen ground based on near-surface meteorological variables, under the assumption that the ground thermal regime is in equilibrium with the applied surface forcing. This is a simplification, and the model cannot reproduce the transient evolution of ground temperatures, and is therefore not suitable for future climate predictions. However, it has proven to capture the regional patterns of permafrost reasonably well (Gisnås et al., 2013; Westermann et al., 2013). Because of the simplicity it is computationally

efficient, and suitable for doing test-studies like the one presented in this paper and in similar studies (Westermann et al., 2015).

For the model evaluation with measured ground temperatures in boreholes (Section 5.4), the modelled temperatures are forced with data for the hydrological year corresponding to the observations. Because of the assumption of an equilibrium situation in the model approach, such a comparison can be problematic as many of the boreholes have undergone warming during the past decades. However, with the majority of the boreholes located in bedrock or coarse moraine material with relatively high conductivity, the lag in the climate signal is relatively small at the ~~depth of the~~ top of permafrost. The lag will also vary from borehole to borehole, depending on the ground thermal properties. Since we use data distributed over larger areas and longer time periods, including a large range of situations, the effect mainly ~~shows in~~ terms of a larger statistical spread and not a systematic error.

The large amount of field observations used for calibration and evaluation in this study is mainly conducted in alpine mountain areas. The large spatial variation in winter snow depths is a major controlling factor also of the ground temperatures in peat plateaus and palsa mires, and is a driving factor in palsa formation (e.g. Seppälä, 2011). The sub-grid effect of snow should therefore also be implemented for mire areas, where comparable data sets are lacking.

## 6.2 Model sensitivity

The sensitivity of $CV_{sd}$-model to the modelled ground temperatures is relatively low, with only 9 % variation in permafrost area, although the performance of the snow distribution scheme varies significantly between the models when evaluated with GPR snow surveys (Table 1). In comparison, a *lognormal* instead of a *gamma* distribution function reduces the permafrost area by 18% (Table 2). The choice of distribution function ~~therefore~~ seems to be of greater importance than the fine tuning of a model for $CV_{sd}$. This result contradicts the conclusions by Luce and Tarboton (2004), which suggest that the parameterization of the distribution function is more important than the choice of distribution model. With a focus on hydrology and snow cover depletion curves, equal importance was given to both the deeper and shallower snow depths in the mentioned study. In contrast, an accurate representation of the shallowest snow depths is crucial for modelling the ground thermal regime. The low thermal conductivity of snow results in a disconnection of ground surface and air temperatures at snow packs thicker than 0.5 – 1 m, depending on the physical properties of

the snow pack and the surface roughness (e.g. Haeberli, 1973). In wind exposed areas prone to heavy redistribution, large fractions of the area will be entirely bare blown (Gisnås et al., 2014). These are the areas of greatest importance for permafrost modelling. In order to reproduce the gradual transition in the discontinuous permafrost zone, where permafrost is often only present at bare blown ridges, shallow snow covers must be satisfactorily represented. Compared to a *gamma* function, a *lognormal* distribution function to a larger degree underestimates the fraction of shallow snow depths, resulting in a less accurate representation of this transition.

Several studies include statistical representations of the sub-grid variability of snow in hydrological models, most commonly applying a two- or three-parameter *lognormal* distribution (e.g. Donald et al., 1995; Liston, 2004; Pomeroy et al., 2004; Nitta et al., 2014). Observed snow distributions within 1x1 km in the ALS snow survey presented in this paper are closer to a *gamma* than to a *lognormal* distribution, supporting the findings by Skaugen (2007) and Winstral and Marks (2014) which were conducted in non-forested alpine environments. However, the difference is not substantial in all areas; the two distributions can provide near-equal fit in eastern parts of the mountain plateau where the terrain is gentler and the wind speeds lower. We suggest that the choice of distribution function of snow is important in model applications for the ground thermal regime, and recommend the use of *gamma* distribution for non-vegetated high alpine areas prone to heavy redistribution of snow.

While a *gamma* distribution offers improvements over a *lognormal* distribution, the bare blown areas are still not sufficiently represented. One attempt to solve this is to include a third parameter for the "snow free fraction" (e.g. Kolberg et al., 2006; Kolberg and Gottschalk, 2010). We made an attempt to calibrate such a parameter for this study, however, no correlations to any of the predictors were found. It is also difficult to determine a threshold depth for "snow free" areas in ALS data resampled to 10 meter resolution, where the uncertainty of the snow depth observations are in the order of ten centimetres (Melvold and Skaugen, 2013).

In this study a high number of realizations could be run per grid cell because of the low computational cost of the model. To evaluate the sensitivity of sampling density, the number of realizations was reduced from 100 to 10 per grid cell. This resulted is a 2.6 % increase in total modelled permafrost area relative to the reference model run. This demonstrates that a

statistical downscaling of ground temperatures as demonstrated in this study is robust and highly improves the model results with only a few additional model realizations per grid cell.

## 7 Conclusions

We present a modelling approach to reproduce the variability of ground temperatures within the scale of 1 km$^2$ grid cells based on probability distribution functions over corresponding seasonal maximum snow depths. The snow distributions are derived from climatic parameters and terrain parameterizations at 10 meter resolution, and are calibrated with a large scale data set of snow depths obtained from laser scanning. The model results are evaluated with independent observations of snow depth distributions, ground surface temperature distributions and ground temperatures. From this study the following conclusions can be drawn:

- The model results indicate a total permafrost area of 25 400 km$^2$, corresponding to 7.8 % of the Norwegian mainland, in an equilibrium situation with the average climate over 1981-2010. 4 % of the model domain features permafrost for all snow depths.
- The same permafrost model without a sub-grid representation of snow produces almost 50 % less permafrost. Because of the non-linearity in the insulating effect of snow cover in combination with the highly asymmetric snow distribution within each grid cell, sub-grid variability of snow depths ~~must be accounted for in models representing~~ the ground thermal regime.
- Observed variations in ground surface temperatures from two logger arrays with 26 and 41 loggers, respectively, are very well reproduced, with estimated fractions of sub-zero *MAGST* within ±10%. 94 % of the observed mean annual temperature at top of permafrost in the boreholes are within the modelled ground temperature range for the corresponding grid cell, and mean modelled temperature of the grid cell reproduces the observations with an accuracy of 1.5°C or better.
- The sensitivity of the model to the coefficient of variation of snow ($CV_{sd}$) is relatively low, compared to the choice of theoretical snow distribution function. ~~However, b~~both are minor effects compared to the effect of running the model without a sub-grid distribution.
- The observed $CV_{sd}$ of snow within 1 km$^2$ grid cells in the Hardangervidda mountain plateau varies from 0.15 to 1.15, with an average $CV_{sd}$ of 0.6. The distributions are

generally closer to a theoretical gamma distribution than to a *lognormal* distribution, in particular in areas of very rough topography, thicker snow cover and higher average winter wind speeds. The observed $CV_{sd}$ values are nearly identical at the end of the accumulation seasons in 2008 and 2009.

In areas subject to snow redistribution, the average ground temperature of a 1 km$^2$ grid cell must be determined based on the distribution, and not the overall average of snow depths within the grid cell. ~~Furthermore, m~~odelling the full range of ground temperatures present over small distances enables representation of the gradual transition from permafrost to non-permafrost areas and most likely a more accurate response to climate warming. This study ~~is~~ clear evidence that the sub-grid variability of snow depths ~~should be accounted for in model approaches targeting the~~ ground thermal regime and permafrost distribution.


## Acknowledgements

This study is part of the CryoMet project (project number 214465; funded by the Norwegian Research Council). The field campaigns at Finse was partly founded by the hydropower companies *Statkraft* and *ECO*, while the field work at Juvvasshøe was done in collaboration with Ketil Isaksen (Norwegian Meteorological Institute). The Norwegian Meteorological Institute provided the NORA10 wind data and the *seNorge* gridded temperature data. The Norwegian Water and Energy Directorate provided the *seNorge* gridded snow depth data and the ALS snow survey at Hardangervidda. Kolbjørn Engeland gave valuable comments to the statistical analysis presented in the manuscript. We gratefully acknowledge the support of all mentioned individuals and institutions.


## References


Aune-Lundberg, L., and Strand, G.-H.: CORINE Land Cover 2006. The Norwegian CLC2006 project, Report from the Norwegian Forest and Landscape Institute: 11/10, 14p, 2010.

Clark, M. P., Hendrikx, J., Slater, A. G., Kavetski, D., Anderson, B., Cullen, N. J., Kerr, T., Hreinsson, E. Ö., and Woods, R. A.: Representing spatial variability of snow water equivalent in hydrologic and land-surface models: A review, Water Resources Research, 47, 10.1029/2011WR010745, 2011.

Donald, J. R., Soulis, E. D., Kouwen, N., and Pietroniro, A.: A Land Cover-Based Snow Cover Representation for Distributed Hydrologic Models, Water Resources Research, 31, 995-1009, 10.1029/94WR02973, 1995.

Dunse, T., Schuler, T. V., Hagen, J. O., Eiken, T., Brandt, O., and Høgda, K. A.: Recent fluctuations in the extent of the firn area of Austfonna, Svalbard, inferred from GPR, Annals of Glaciology, 50, 155-162, 10.3189/172756409787769780, 2009.

Engeset, R., Tveito, O. E., Alfnes, E., Mengistu, Z., Udnæs, C., Isaksen, K., and Førland, E. J.: Snow map System for Norway., XXIII Nordic Hydrological Conference, 8-12 Aug., Tallin, Estonia. NHP Report: 48(1), 2004,

Farbrot, H., Isaksen, K., and Etzelmüller, B.: Present and past distribution of mountain permafrost in Gaissane Mountains, Northern Norway, In: Proceeding of the Ninth International Conference on Permafrost, Fairbanks, Alaska, 2008, 427–432,

Farbrot, H., Hipp, T. F., Etzelmüller, B., Isaksen, K., Ødegård, R. S., Schuler, T. V., and Humlum, O.: Air and Ground Temperature Variations Observed along Elevation and Continentality Gradients in Southern Norway, Permafrost and Periglacial Processes, 22, 343-360, 10.1002/ppp.733, 2011.

Farbrot, H., Isaksen, K., Etzelmüller, B., and Gisnås, K.: Ground Thermal Regime and Permafrost Distribution under a Changing Climate in Northern Norway, Permafrost and Periglacial Processes, 24, 20-38, 10.1002/ppp.1763, 2013.

Fiddes, J., and Gruber, S.: TopoSUB: a tool for efficient large area numerical modelling in complex topography at sub-grid scales, Geosci. Model Dev., 5, 1245-1257, 10.5194/gmd-5-1245-2012, 2012.

Gisnås, K., Etzelmuller, B., Farbrot, H., Schuler, T. V., and Westermann, S.: CryoGRID 1.0: Permafrost Distribution in Norway estimated by a Spatial Numerical Model, Permafrost and Periglacial Processes, 24, 2-19, 10.1002/ppp.1765, 2013.

Gisnås, K., Westermann, S., Schuler, T. V., Litherland, T., Isaksen, K., Boike, J., and Etzelmüller, B.: A statistical approach to represent small-scale variability of permafrost temperatures due to snow cover, The Cryosphere, 8, 2063-2074, 10.5194/tc-8-2063-2014, 2014.

Goodrich, L. E.: The influence of snow cover on the ground thermal regime, Can. Geotech. J., 19, 421-432, 1982.

Gruber, S., and Haeberli, W.: Mountain permafrost, in: Permafrost Soils, edited by: Margesin, R., Springer, 33-44, 2009.

Gubler, H., Fiddes, J., Gruber, S., and Keller, M.: Scale-dependent measurement and analysis of ground surface temperature variability in alpine terrain, The Cryosphere, 5, 307-338, 10.5194/tcd-5-307-2011, 2011.

Haakenstad, H., Reistad, M., Haugen, J. E., and Breivik, Ø.: Update of the NORA10 hindcast archive for 2011 and study of polar low cases with the WRF model, met.no report 17/2012, Oslo, 2012.

Haeberli, W.: Die Basis-Temperatur der winterlichen Schneedecke als möglicher Indikator für die Verbreitung von Permafrost in den Alpen, Zeitschrift für Gletscherkunde und Glazialgeologie, 9, 221-227, 1973.

Hipp, T.: Mountain Permafrost in Southern Norway. Distribution, Spatial Variability and Impacts of Climate Change., PhD, Faculty of Mathematics and Natural Sciences, Department of Geosciences, University of Oslo, 166 pp., 2012.

Isaksen, K., Hauck, C., Gudevang, E., Ødegård, R. S., and Sollid, J. L.: Mountain permafrost distribution in Dovrefjell and Jotunheimen, southern Norway, based on BTS and DC resistivity tomography data, Norsk Geografisk Tidsskrift-Norwegian Journal of Geography, 56, 122-136, 10.1080/00291950276005645 9, 2002.

Isaksen, K., Sollid, J. L., Holmlund, P., and Harris, C.: Recent warming of mountain permafrost in Svalbard and Scandinavia, Journal of Geophysical Research., 112, F02S04, 10.1029/2006jf000522, 2007.

Isaksen, K., Farbrot, H., Blikra, L., Johansen, B., Sollid, J., and Eiken, T.: Five year ground surface temperature measurements in Finnmark, Northern Norway., Ninth International Conference on Permafrost, Fairbanks, Alaska, 2008, 789–794,

Isaksen, K., Ødegård, R. S., Etzelmüller, B., Hilbich, C., Hauck, C., Farbrot, H., Eiken, T., Hygen, H. O., and Hipp, T. F.: Degrading Mountain Permafrost in Southern Norway: Spatial and Temporal Variability of Mean Ground Temperatures, 1999–2009, Permafrost and Periglacial Processes, 22, 361-377, 10.1002/ppp.728, 2011.

Kolberg, S., Rue, H., and Gottschalk, L.: A Bayesian spatial assimilation scheme for snow coverage observations in a gridded snow model, Hydrol. Earth Syst. Sci., 10, 369-381, 10.5194/hess-10-369-2006, 2006.

Kolberg, S., and Gottschalk, L.: Interannual stability of grid cell snow depletion curves as estimated from MODIS images, Water Resources Research, 46, n/a-n/a, 10.1029/2008WR007617, 2010.

Kolberg, S. A., and Gottschalk, L.: Updating of snow depletion curve with remote sensing data, Hydrological Processes, 20, 2363-2380, 2006.

Kovacs, A., Gow, A. J., and Morey, R. M.: The in-situ dielectric constant of polar firn revisited, Cold Regions Science and Technology, 23, 245-256, 10.1016/0165-232X(94)00016-Q, 1995.

Langer, M., Westermann, S., Heikenfeld, M., Dorn, W., and Boike, J.: Satellite-based modeling of permafrost temperatures in a tundra lowland landscape, Remote Sensing of Environment, 135, 12-24, 10.1016/j.rse.2013.03.011, 2013.

Lehning, M., and Fierz, C.: Assessment of snow transport in avalanche terrain, Cold Regions Science and Technology, 51, 240-252, 10.1016/j.coldregions.2007.05.012, 2008.

Lewkowicz, A. G., and Ednie, M.: Probability mapping of mountain permafrost using the BTS method, Wolf Creek, Yukon Territory, Canada, Permafrost and Periglacial Processes, 15, 67-80, 10.1002/ppp.480, 2004.

Li, L., and Pomeroy, J. W.: Estimates of Threshold Wind Speeds for Snow Transport Using Meteorological Data, Journal of Applied Meteorology, 36, 205-213, 10.1175/1520-0450(1997)036<0205:EOTWSF>2.0.CO;2, 1997.

Liston, G. E.: Representing Subgrid Snow Cover Heterogeneities in Regional and Global Models, Journal of Climate, 17, 1381-1397, 10.1175/1520-0442(2004)017<1381:RSSCHI>2.0.CO;2, 2004.

Luce, C. H., and Tarboton, D. G.: The application of depletion curves for parameterization of subgrid variability of snow, Hydrological Processes, 18, 1409-1422, 10.1002/hyp.1420, 2004.

Lussana, C., Uboldi, F., and Salvati, M. R.: A spatial consistency test for surface observations from mesoscale meteorological networks, Quarterly Journal of the Royal Meteorological Society, 136, 1075-1088, 10.1002/qj.622, 2010.

Melvold, K., and Skaugen, T.: Multiscale spatial variability of lidar-derived and modeled snow depth on Hardangervidda, Norway, Annals of Glaciology, 54, 273-281, 10.3189/2013AoG62A161, 2013.

Nitta, T., Yoshimura, K., Takata, K., O'ishi, R., Sueyoshi, T., Kanae, S., Oki, T., Abe-Ouchi, A., and Liston, G. E.: Representing Variability in Subgrid Snow Cover and Snow Depth in a Global Land Model: Offline Validation, Journal of Climate, 27, 3318-3330, 10.1175/JCLI-D-13-00310.1, 2014.

Pomeroy, J., Essery, R., and Toth, B.: Implications of spatial distributions of snow mass and melt rate for snow-cover depletion: observations in a subarctic mountain catchment, Annals of Glaciology, 38, 195-201, 10.3189/172756404781814744, 2004.

Reistad, M., Breivik, Ø., Haakenstad, H., Aarnes, O. J., Furevik, B. R., and Bidlot, J.-R.: A high-resolution hindcast of wind and waves for the North Sea, the Norwegian Sea, and the Barents Sea, Journal of Geophysical Research: Oceans, 116, C05019, 10.1029/2010JC006402, 2011.

Saloranta, T. M.: Simulating snow maps for Norway: description and statistical evaluation of the seNorge snow model, The Cryosphere, 6, 1323-1337, 10.5194/tc-6-1323-2012, 2012.

Seppälä, M.: Synthesis of studies of palsa formation underlining the importance of local environmental and physical characteristics, Quaternary Research, 75, 366-370, http://dx.doi.org/10.1016/j.yqres.2010.09.007, 2011.

Skaugen, T., Alfnes, E., Langsholt, E. G., and Udnæs, H.-C.: Time-variant snow distribution for use in hydrological models, Annals of Glaciology, 38, 180-186, 10.3189/172756404781815013, 2004.

Skaugen, T.: Modelling the spatial variability of snow water equivalent at the catchment scale, Hydrol. Earth Syst. Sci., 11, 1543-1550, 10.5194/hess-11-1543-2007, 2007.

Stephens, M. A.: EDF Statistics for Goodness of Fit and Some Comparisons, Journal of the American Statistical Association, 69, 730-737, 10.1080/01621459.1974.10480196, 1974.

Westermann, S., Schuler, T. V., Gisnås, K., and Etzelmüller, B.: Transient thermal modeling of permafrost conditions in Southern Norway, The Cryosphere, 7, 719-739, 10.5194/tc-7-719-2013, 2013.

Westermann, S., Østby, T., Gisnås, K., Schuler, T. V., and Etzelmüller, B.: A ground temperature map of the North Atlantic permafrost region based on remote sensing and reanalysis data, The Cryosphere Discuss., 9, 753-790, 10.5194/tcd-9-753-2015, 2015.

Winstral, A., Elder, K., and Davis, R. E.: Spatial snow modeling of wind-redistributed snow using terrain-based parameters, Journal of Hydrometeorology, 3, 524-538, http://dx.doi.org/10.1175/1525-7541(2002)003<0524:SSMOWR>2.0.CO;2, 2002.

Winstral, A., and Marks, D.: Long-term snow distribution observations in a mountain catchment: Assessing variability, time stability, and the representativeness of an index site, Water Resources Research, 50, 293-305, 10.1002/2012WR013038, 2014.

Zhang, T., Barry, R. G., and Haeberli, W.: Numerical simulations of the influence of the seasonal snow cover on the occurrence of permafrost at high latitudes, Norsk Geografisk

1 Tidsskrift - Norwegian Journal of Geography, 55, 261-266, 10.1080/00291950152746621,
2 2001.

3 Ødegaard, R. S., Isaksen, K., Eiken, T., and Sollid, J. L.: MAGST in Mountain Permafrost,
4 Dovrefjell, Southern Nroway, 2001-2006, Ninth International Conference on Permafrost
5 (NICOP) 2008, Fairbanks, Alaska, June 29 - July 3, 2008.

6

**Figures:**

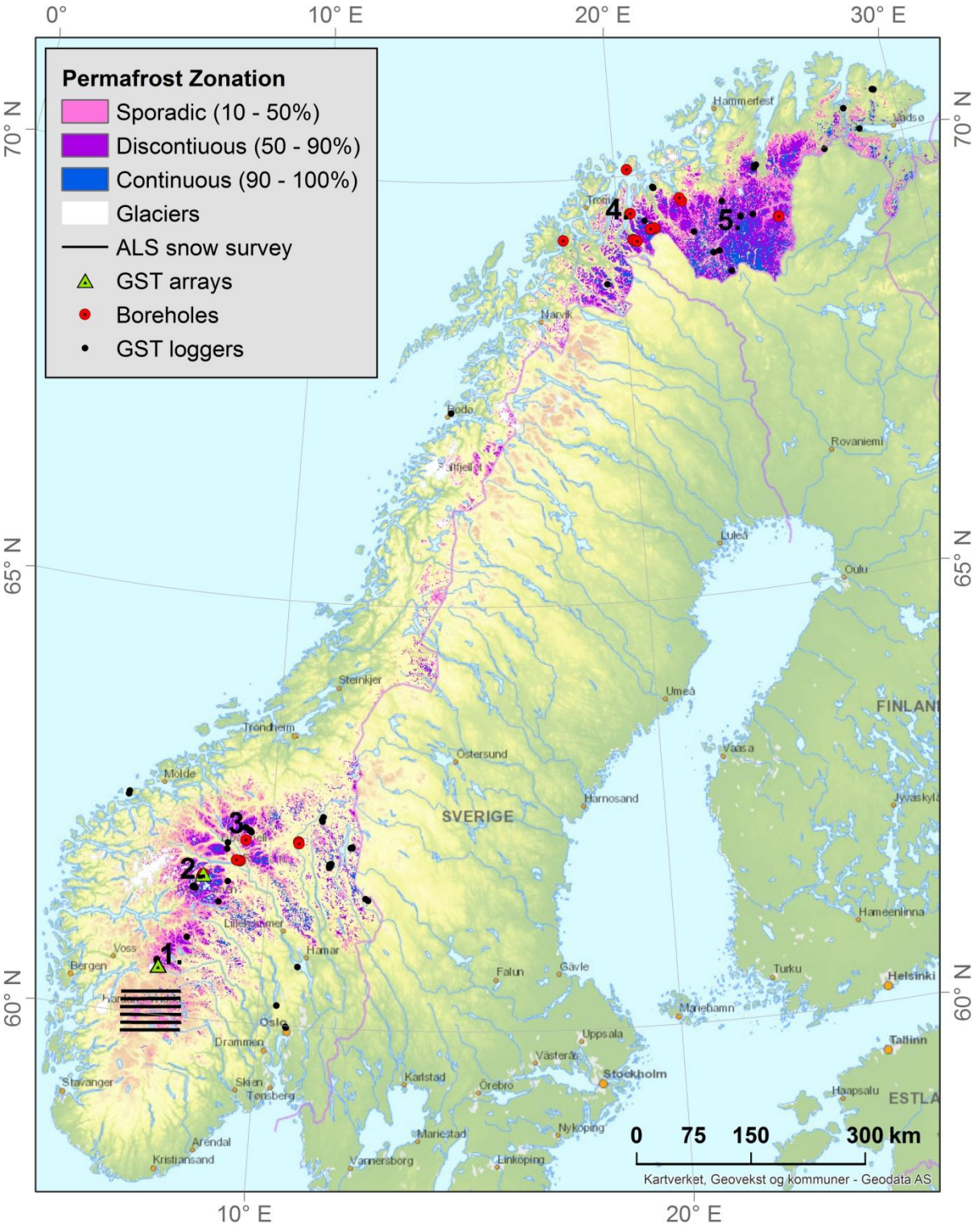


Fig. 1: Modelled distribution of permafrost in Norway. Sites mentioned in the text: 1) Finse, south of Hallingskarvet, 2) Juvvasshøe in Jotunheimen, 3) Dovrefjell, 4) The Lyngen Alps and 5) Finnmark.

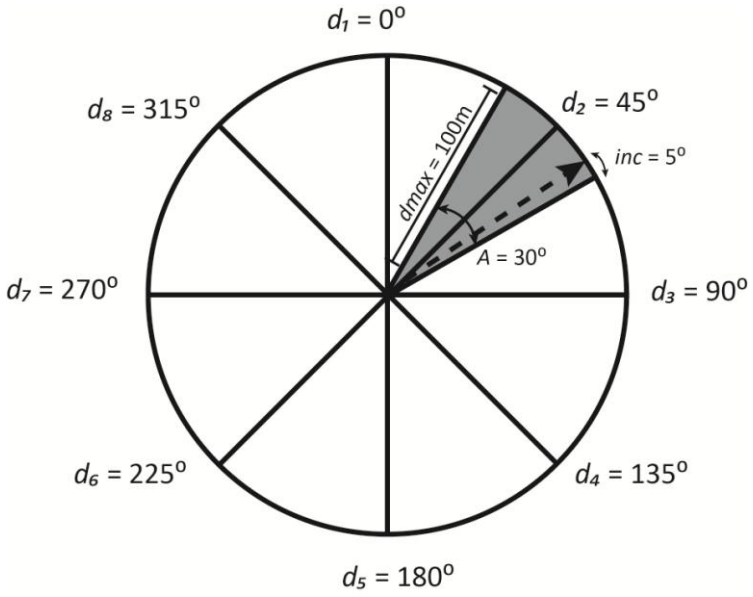


Fig. 2: ~~The figure illustrates the~~ area accounted for in each of the 8 runs of the Winstral terrain-based parameter, each of them with a prevailing wind direction $d_n$. The area accounted for when calculating the exposure of a grid cell is constrained by the search window (*A*) and the search distance *dmax* being 100 meters upwind.

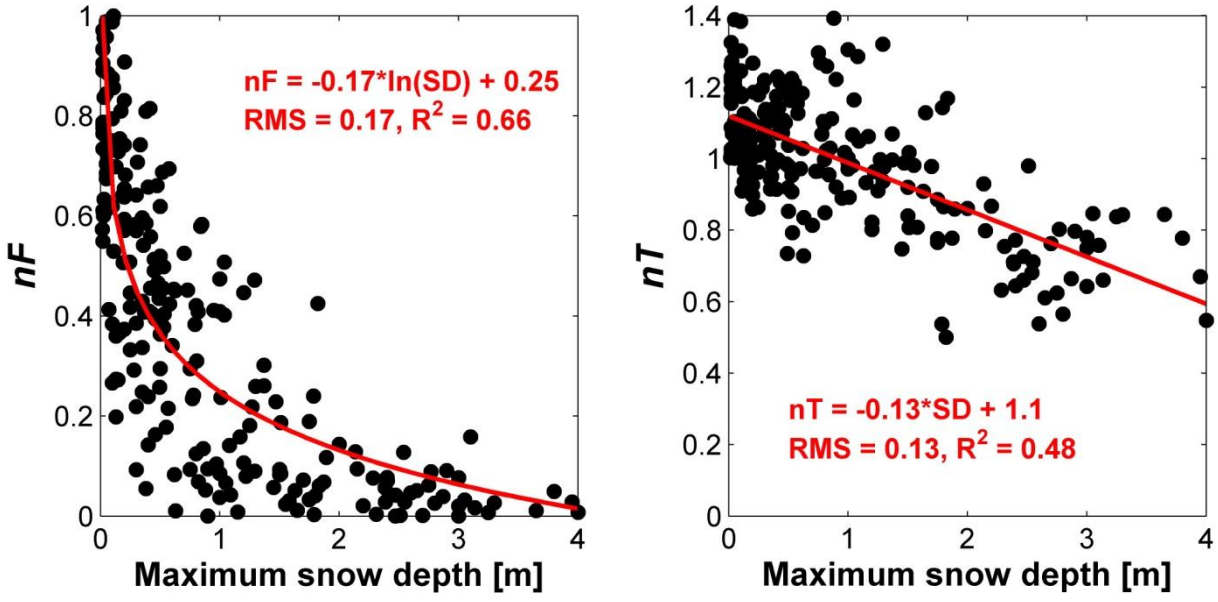


Fig. 3: *nF* and *nT* related to maximum snow depth observed at more than 90 sites located above 1000 m a.s.l. in southern Norway.

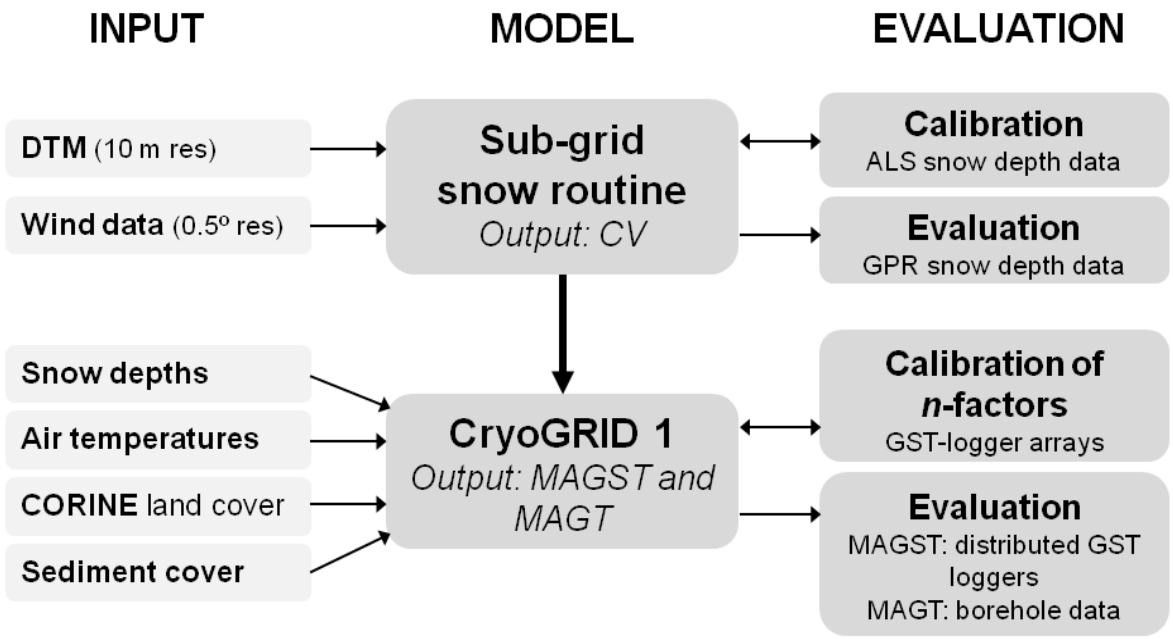


Fig. 4: Schematic of the model chain, including input data and calibration and evaluation procedures.

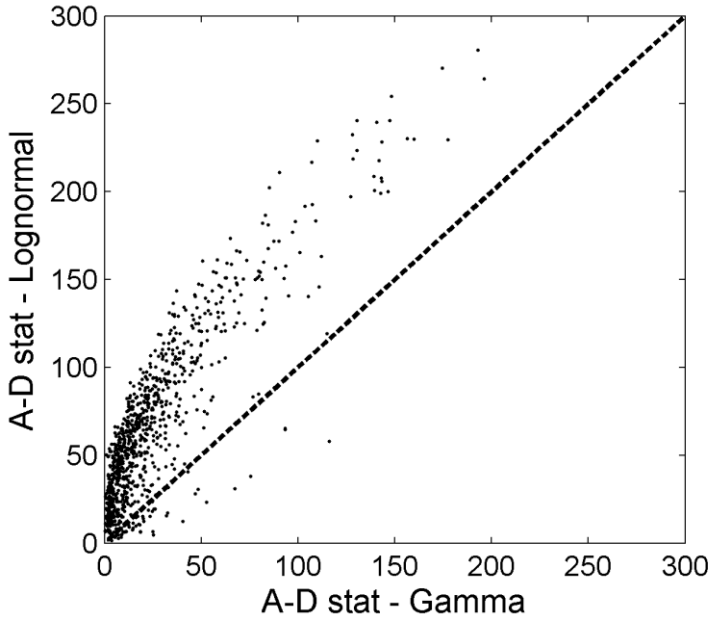


Fig. 5: Scores from the Anderson-Darling Test Statistics for Goodness-of-Fit between theoretical *gamma* and *lognormal* distributions and the observed distribution within each 1x1 km area in the ALS snow survey. Lower scores indicate better fit.

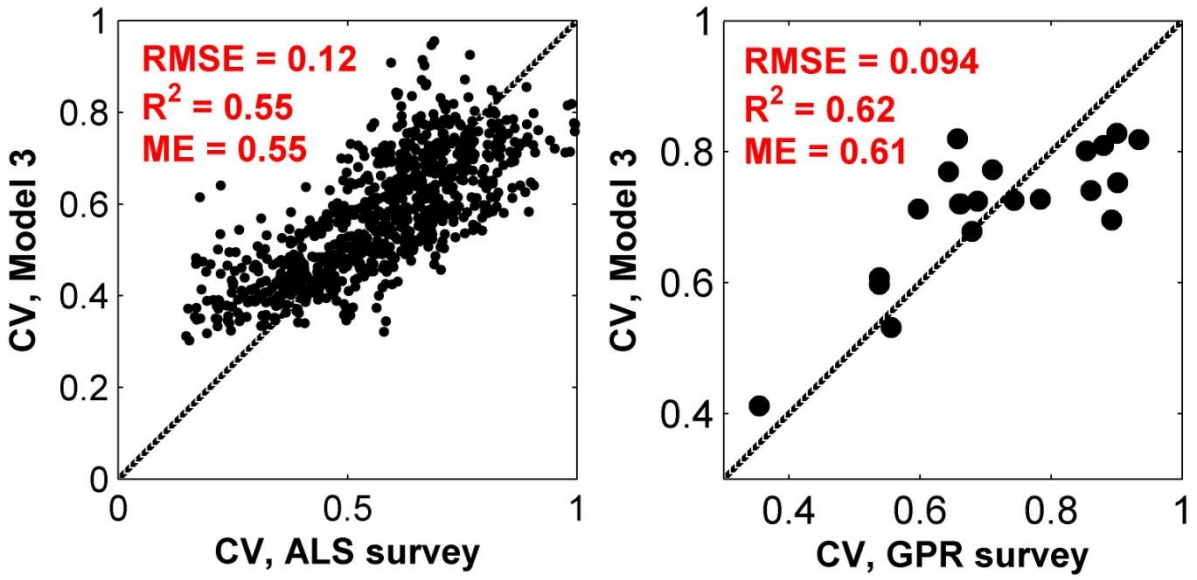


Fig. 6: Left: Fit ~~for~~ the regression *Model 3* for $CV_{sd}$, calibrated with $CV_{sd}$ derived from the ALS snow survey. Right: The model performance is evaluated with independent ground penetrating radar (GPR) snow surveys from at Finse and Juvvasshøe.

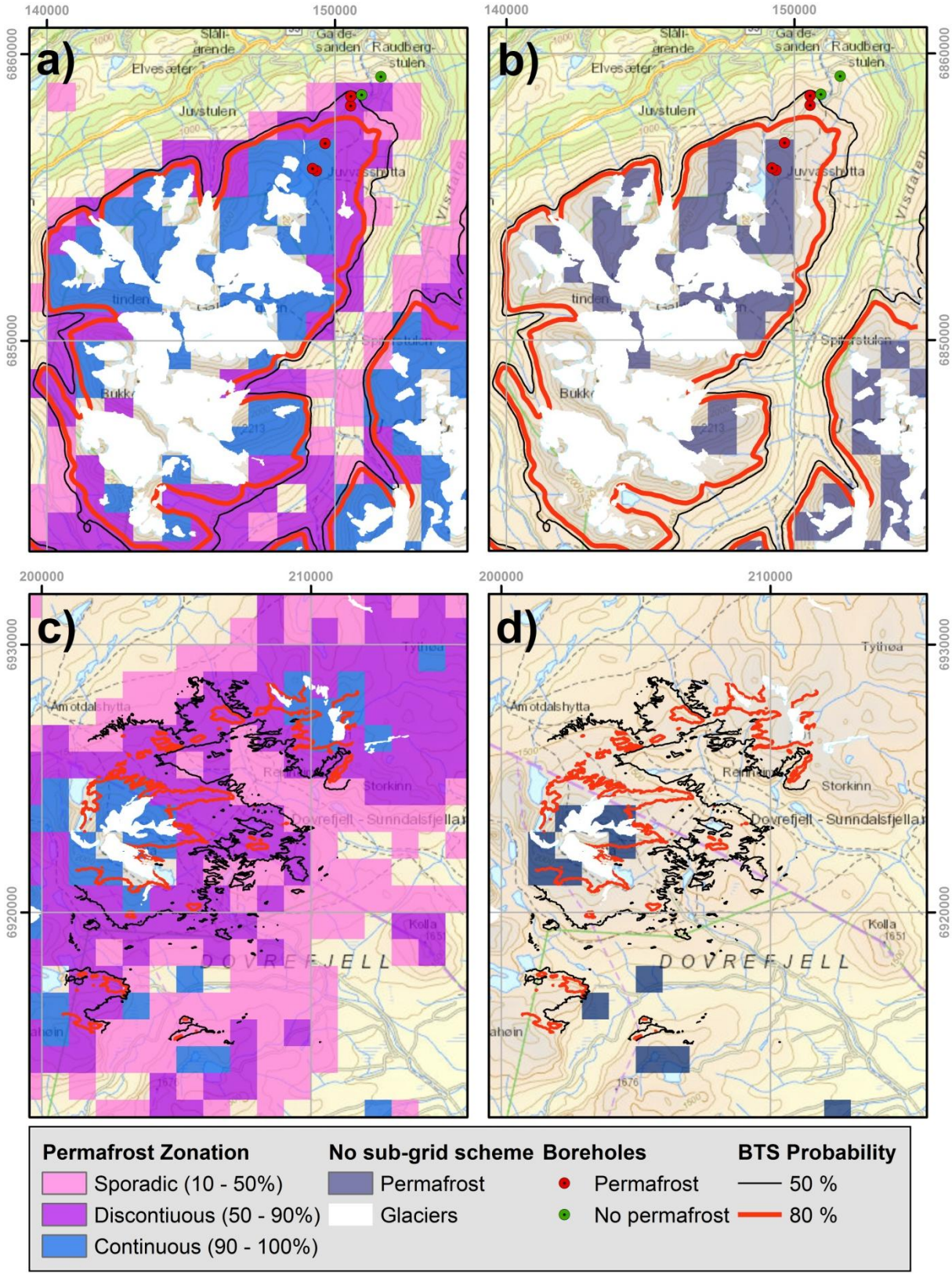


Fig. 7: Distribution of permafrost at Juvvasshøe in Jotunheimen (a and b), and at Dovrefjell (c and d) modelled as permafrost zones applying the sub-grid approach (left) compared to the modelled mean annual ground temperature (*MAGT*) without a sub-grid approach (right).

Lower limit of 50 % and 80 % probability of permafrost derived from BTS-surveys are shown as black and red contour lines, respectively. Borehole locations with permafrost (red) and seasonal frost (green) are shown as dots in the map at Juvvasshøe.

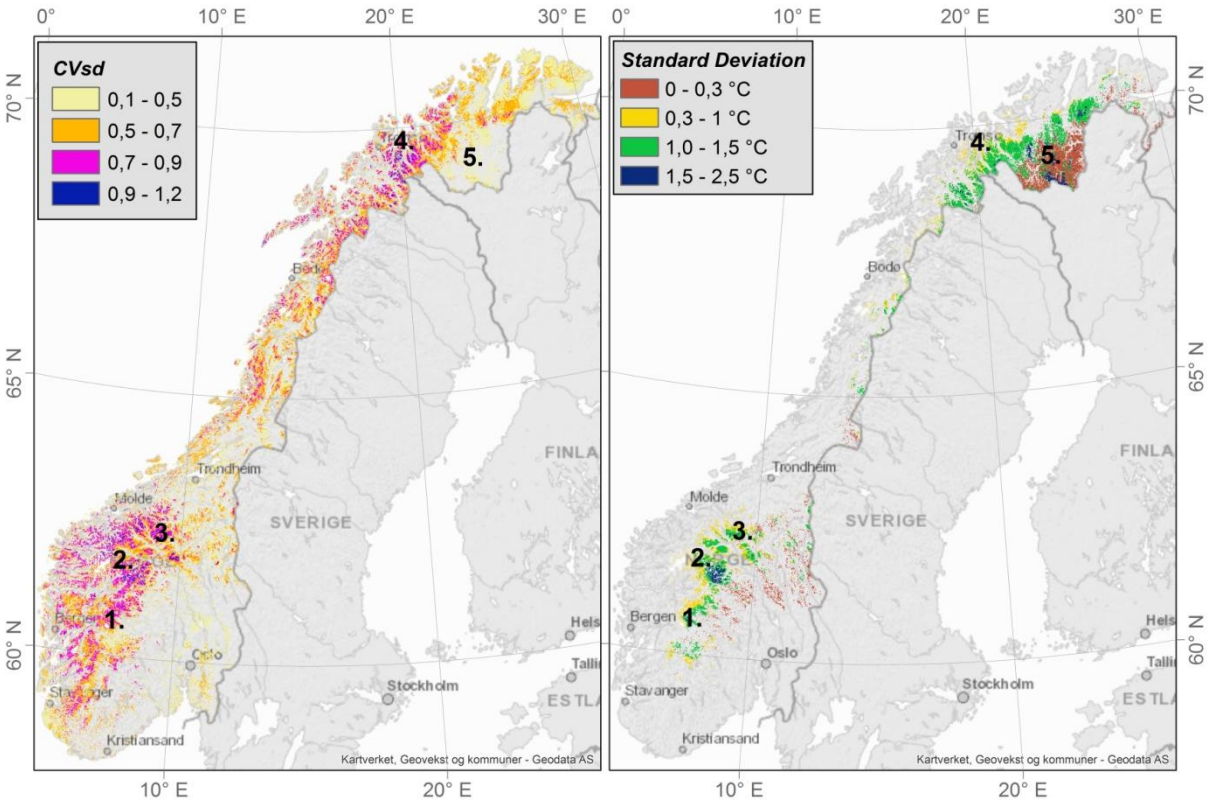


Fig. 8: Left: Distribution of modelled $CV_{sd}$ in non-vegetated areas of Norway with *Model 3*. $CV_{sd}$ increases in areas of rougher topography (western side of Norway) and higher elevations (central part following the Scandes). Right: Standard deviation of modelled *MAGT* for areas of modelled permafrost. Sites mentioned in the text: 1) Finse, south of Hallingskarvet, 2) Juvvasshøe in Jotunheimen, 3) Dovrefjell, 4) The Lyngen Alps and 5) Finnmark.

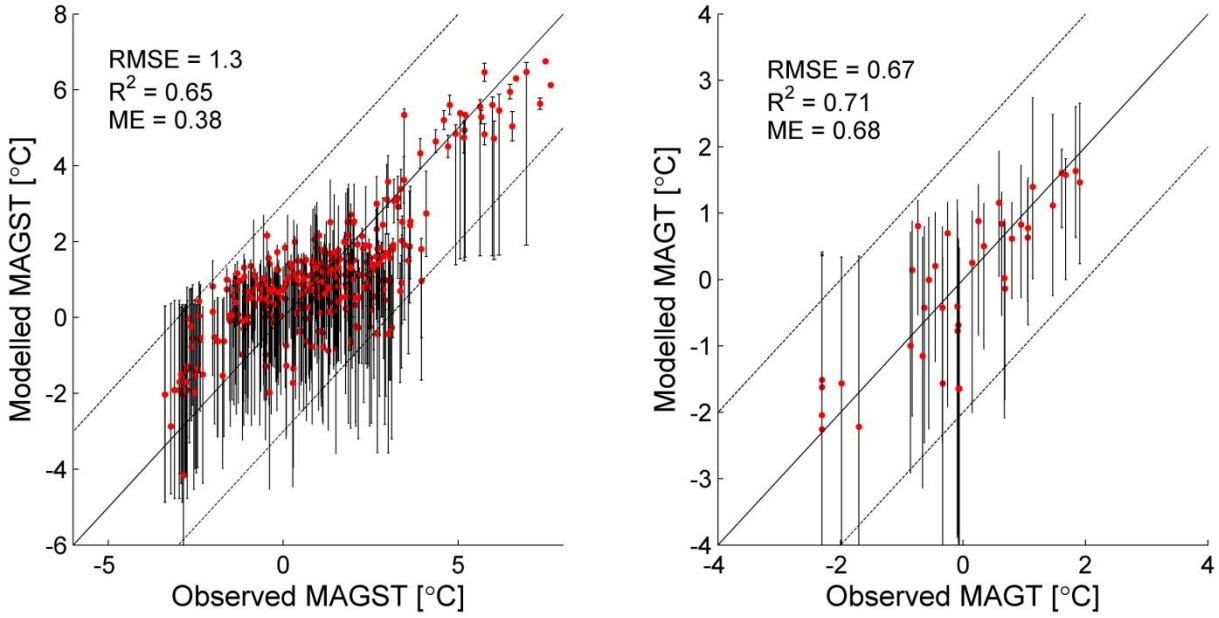


Fig. 9: ~~The figure shows the c~~orrelation between modelled and observed *MAGST* (left) and *MAGT* at the top of permafrost (right). The dotted line indicates ± 2 °C of the 1:1 line (black line). The vertical bars indicate the variation of modelled temperatures within the grid cell, and the red dots indicates the mean temperature.

## Tables:

Table 1: The three regression models for $CV_{sd}$ with in increasing number of predictors are calibrated with observed snow distributions from the ALS snow survey (left columns). P-values are < $10^{-6}$. The isolated snow distribution scheme is validated with independent snow distribution data collected with GPR snow surveys (right columns). Root mean square error (*RMSE*), coefficient of determination ($R^2$) and Nash-Sutcliffe model efficiency (*ME*) are given for each model evaluation.

| 8 | $CV_{sd}$ = | Fit of regression | | | $CV_{sd}$, GPR survey | | |
|---|---|---|---|---|---|---|---|
| | | *RMSE* | $R^2$ | *ME* | *RMSE* | $R^2$ | *ME* |
| ***Model 1*** | $0.39 + 3.4*CV_{Sx}$ | 0.14 | 0.36 | 0.36 | 0.20 | 0.04 | -0.71 |
| ***Model 2*** | $0.31 + 3.1*CV_{Sx} + 4.05e\text{-}4*z$ | 0.12 | 0.52 | 0.52 | 0.12 | 0.59 | 0.36 |
| ***Model 3*** | $0.40 + 3.1*CV_{Sx} + 4.95e\text{-}04*z - 0.0713*\mu$ | 0.12 | 0.55 | 0.55 | 0.09 | 0.62 | 0.61 |

Table 2: The model performance is evaluated with respect to the mean annual ground surface temperatures (*MAGST*) and the mean annual temperature at the depth of the active layer or seasonal freezing layer (*MAGT*). Modelled average *MAGST* or *MAGT* over a grid cell is compared to more than 100 GST logger locations and 25 boreholes. The location of the GST loggers and boreholes are shown in Fig. 1. Modelled permafrost distribution is given in total areas, and as percentage of the model domain, corresponding to the Norwegian mainland area.

| | | **Permafrost model evaluation** | | | | | | **Modelled permafrost area** | |
|---|---|---|---|---|---|---|---|---|---|
| | | MAGST, GST loggers | | | MAGT, boreholes | | | | |
| | | *RMSE* | $R^2$ | *ME* | *RMSE* | $R^2$ | *ME* | *[km²]* | *[%]* |
| **No sub-grid variation** | | 1.57 | 0.65 | -0.56 | 1.19 | 0.62 | -1.90 | 13 462 | 4.1 |
| **GAMMA** | **$CV_{sd}$ = 0.6** | 1.37 | 0.64 | 0.06 | 0.77 | 0.66 | 0.22 | 23 571 | 7.3 |
| | ***Model 1*** | 1.36 | 0.63 | 0.12 | 0.77 | 0.66 | 0.11 | 23 147 | 7.1 |
| | ***Model 2*** | 1.29 | 0.65 | 0.31 | 0.65 | 0.71 | 0.62 | 23 674 | 7.3 |
| | ***Model 3**** | **1.29** | **0.65** | **0.38** | **0.67** | **0.71** | **0.68** | **25 407** | **7.8** |
| **LOGN** | ***Model 1*** | 1.40 | 0.64 | -0.06 | 0.87 | 0.67 | -0.25 | 19 975 | 6.2 |
| | ***Model 2*** | 1.38 | 0.65 | 0.01 | 0.82 | 0.69 | 0.09 | 20 067 | 6.2 |
| | ***Model 3*** | 1.36 | 0.65 | 0.06 | 0.78 | 0.69 | 0.22 | 20 889 | 6.2 |

*Reference model run.

Table 3: Observed and modelled values for the coefficient of variation for maximum snow depth ($CV_{sd}$) and spatial distributions of Mean Annual Ground Surface Temperatures (MAGST) at the field sites at Finse and Juvvasshøe. The MAGST modelled without a sub-grid distribution of snow is given in parenthesis.

| | **Juvvasshøe** | | **Finse** | |
|---|---|---|---|---|
| | Observed | Modelled | Observed | Modelled |
| **$CV_{sd}$** | 0.85 | 0.80 | 0.71 | 0.77 |
| **MAGST < 0 °C** | 77 % | 64 % | 30 % | 32 % |
| **$MAGST_{min}$** | -1.8 °C | -2.6 °C | -1.9 °C | -1.6 °C |
| **$MAGST_{max}$** | 1.0 °C | 0.8 °C | 2.7 °C | 1.0 °C |
| **$MAGST_{avg}$** | -0.5 °C | -0.5 °C (0.8 °C) | 0.8 °C | 0.2 °C (1.3 °C) |

## Supplementary material

Table S1: Location, vegetation type and period of measurements of ground surface temperature loggers used for validation.

| Latitude | Longitude | Elevation (m) | Vegetation type | Start Year | End Year | No. Years |
|---|---|---|---|---|---|---|
| 62.543 | 6.303 | 92 | Forest | 2005 | 2008 | 3 |
| 62.575 | 6.317 | 796 | Non-vegetated | 2005 | 2006 | 1 |
| 62.297 | 9.338 | 1505 | Non-vegetated | 2001 | 2007 | 6 |
| 62.296 | 9.354 | 1467 | Non-vegetated | 2001 | 2004 | 3 |
| 62.264 | 9.467 | 1094 | Non-vegetated | 2002 | 2007 | 5 |
| 62.247 | 9.499 | 1039 | Non-vegetated | 2002 | 2007 | 5 |
| 61.522 | 12.504 | 541 | Forest | 2005 | 2008 | 3 |
| 61.542 | 12.439 | 1022 | Non-vegetated | 2005 | 2008 | 3 |
| 60.593 | 7.526 | 1210 | Non-vegetated | 2006 | 2007 | 1 |
| 60.651 | 7.493 | 1559 | Non-vegetated | 2006 | 2007 | 1 |
| 60.632 | 7.496 | 1431 | Non-vegetated | 2006 | 2007 | 1 |
| 60.647 | 7.489 | 1508 | Non-vegetated | 2006 | 2007 | 1 |
| 60.948 | 8.152 | 1220 | Non-vegetated | 2005 | 2007 | 2 |
| 62.429 | 11.274 | 1538 | Non-vegetated | 2004 | 2007 | 3 |
| 62.480 | 11.293 | 676 | Forest | 2006 | 2008 | 2 |
| 62.447 | 11.261 | 1251 | Non-vegetated | 2006 | 2008 | 2 |
| 61.721 | 8.401 | 1065 | Non-vegetated | 2004 | 2007 | 3 |
| 61.707 | 8.403 | 1307 | Non-vegetated | 1999 | 2007 | 8 |
| 61.702 | 8.395 | 1391 | Non-vegetated | 1999 | 2002 | 3 |
| 61.702 | 8.394 | 1410 | Non-vegetated | 1999 | 2002 | 3 |
| 61.701 | 8.393 | 1430 | Non-vegetated | 1999 | 2002 | 3 |
| 61.701 | 8.393 | 1447 | Non-vegetated | 1999 | 2008 | 9 |
| 61.699 | 8.391 | 1480 | Non-vegetated | 1999 | 2001 | 2 |
| 61.699 | 8.390 | 1492 | Non-vegetated | 1999 | 2000 | 1 |
| 61.685 | 8.376 | 1767 | Non-vegetated | 2004 | 2007 | 3 |
| 61.678 | 8.369 | 1893 | Non-vegetated | 1999 | 2004 | 5 |
| 61.677 | 8.369 | 1893 | Non-vegetated | 1999 | 2007 | 8 |
| 61.678 | 8.369 | 1893 | Non-vegetated | 1999 | 2004 | 5 |
| 61.649 | 9.012 | 855 | Forest | 2005 | 2008 | 3 |

| | | | | | | |
|---|---|---|---|---|---|---|
| 61.401 | 8.831 | 1525 | Non-vegetated | 2005 | 2007 | 2 |
| 61.555 | 8.193 | 1522 | Non-vegetated | 2005 | 2007 | 2 |
| 61.556 | 8.207 | 1389 | Non-vegetated | 2005 | 2007 | 2 |
| 61.552 | 8.182 | 1460 | Non-vegetated | 2006 | 2007 | 1 |
| 61.547 | 8.163 | 1354 | Non-vegetated | 2006 | 2007 | 1 |
| 61.532 | 8.230 | 1448 | Non-vegetated | 2006 | 2007 | 1 |
| 61.538 | 8.180 | 1696 | Non-vegetated | 2006 | 2007 | 1 |
| 62.099 | 8.931 | 607 | Forest | 2005 | 2008 | 3 |
| 62.027 | 8.925 | 1573 | Non-vegetated | 2004 | 2008 | 4 |
| 59.989 | 10.670 | 528 | Forest | 2003 | 2006 | 3 |
| 59.980 | 10.683 | 443 | Forest | 2004 | 2008 | 4 |
| 59.980 | 10.684 | 435 | Forest | 2004 | 2008 | 4 |
| 60.232 | 10.428 | 196 | Forest | 2006 | 2008 | 2 |
| 61.934 | 11.548 | 805 | Non-vegetated | 2002 | 2003 | 1 |
| 61.931 | 11.543 | 868 | Non-vegetated | 2002 | 2006 | 4 |
| 61.930 | 11.542 | 918 | Non-vegetated | 2002 | 2006 | 4 |
| 61.927 | 11.540 | 1010 | Non-vegetated | 2002 | 2006 | 4 |
| 61.925 | 11.538 | 1109 | Non-vegetated | 2002 | 2006 | 4 |
| 61.922 | 11.507 | 987 | Non-vegetated | 2002 | 2006 | 4 |
| 61.926 | 11.511 | 1051 | Non-vegetated | 2002 | 2006 | 4 |
| 61.919 | 11.536 | 1211 | Non-vegetated | 2002 | 2006 | 4 |
| 61.929 | 11.527 | 1043 | Non-vegetated | 2002 | 2003 | 1 |
| 61.929 | 11.527 | 1043 | Non-vegetated | 2002 | 2006 | 4 |
| 61.902 | 11.500 | 1069 | Non-vegetated | 2004 | 2005 | 1 |
| 61.892 | 11.504 | 1078 | Non-vegetated | 2004 | 2005 | 1 |
| 61.926 | 11.535 | 1071 | Non-vegetated | 2004 | 2005 | 1 |
| 61.926 | 11.535 | 1071 | Non-vegetated | 2004 | 2005 | 1 |
| 61.908 | 11.537 | 1418 | Non-vegetated | 2004 | 2005 | 1 |
| 61.908 | 11.537 | 1418 | Non-vegetated | 2004 | 2007 | 3 |
| 61.929 | 11.527 | 1043 | Non-vegetated | 2005 | 2007 | 2 |
| 62.134 | 12.020 | 906 | Shrubs | 2002 | 2006 | 4 |
| 62.135 | 12.055 | 1196 | Non-vegetated | 2002 | 2006 | 4 |
| 62.140 | 12.060 | 1316 | Non-vegetated | 2002 | 2003 | 1 |

| | | | | | | |
|---|---|---|---|---|---|---|
| 62.137 | 12.053 | 1207 | Non-vegetated | 2002 | 2006 | 4 |
| 62.138 | 12.051 | 1192 | Non-vegetated | 2002 | 2006 | 4 |
| 62.137 | 12.030 | 1052 | Non-vegetated | 2002 | 2006 | 4 |
| 62.140 | 12.060 | 1316 | Non-vegetated | 2004 | 2007 | 3 |
| 62.141 | 12.061 | 1335 | Non-vegetated | 2005 | 2007 | 2 |
| 69.942 | 24.862 | 508 | Non-vegetated | 2003 | 2005 | 2 |
| 69.937 | 24.854 | 614 | Non-vegetated | 2003 | 2005 | 2 |
| 69.913 | 24.775 | 1002 | Non-vegetated | 2003 | 2005 | 2 |
| 69.910 | 24.770 | 1034 | Non-vegetated | 2003 | 2005 | 2 |
| 69.909 | 24.771 | 982 | Non-vegetated | 2003 | 2005 | 2 |
| 69.933 | 24.789 | 471 | Non-vegetated | 2004 | 2005 | 1 |
| 69.933 | 24.792 | 428 | Non-vegetated | 2004 | 2005 | 1 |
| 70.075 | 20.431 | 839 | Non-vegetated | 2003 | 2006 | 3 |
| 70.063 | 20.451 | 476 | Non-vegetated | 2003 | 2005 | 2 |
| 69.831 | 21.279 | 895 | Non-vegetated | 2002 | 2008 | 6 |
| 69.838 | 21.273 | 700 | Non-vegetated | 2002 | 2007 | 5 |
| 69.843 | 21.259 | 500 | Non-vegetated | 2002 | 2007 | 5 |
| 69.563 | 20.433 | 861 | Non-vegetated | 2002 | 2007 | 5 |
| 69.576 | 20.437 | 685 | Non-vegetated | 2002 | 2005 | 3 |
| 69.583 | 20.435 | 500 | Non-vegetated | 2002 | 2005 | 3 |
| 69.457 | 20.882 | 966 | Non-vegetated | 2006 | 2007 | 1 |
| 69.354 | 21.211 | 786 | Non-vegetated | 2004 | 2007 | 3 |
| 69.267 | 22.481 | 739 | Non-vegetated | 2003 | 2010 | 7 |
| 69.008 | 23.235 | 355 | Forest | 2003 | 2010 | 7 |
| 69.980 | 27.269 | 130 | Forest | 2003 | 2009 | 6 |
| 70.542 | 29.322 | 502 | Non-vegetated | 2002 | 2009 | 7 |
| 70.541 | 29.342 | 480 | Non-vegetated | 2002 | 2009 | 7 |
| 70.538 | 29.363 | 415 | Non-vegetated | 2002 | 2009 | 7 |
| 70.537 | 29.380 | 355 | Non-vegetated | 2002 | 2009 | 7 |
| 70.400 | 28.200 | 10 | Shrubs | 2008 | 2010 | 2 |
| 70.126 | 28.593 | 50 | Mire | 2008 | 2010 | 2 |
| 69.376 | 24.496 | 284 | Non-vegetated | 2008 | 2010 | 2 |
| 69.370 | 24.082 | 469 | Non-vegetated | 2008 | 2010 | 2 |

| | | | | | | |
|---|---|---|---|---|---|---|
| 69.377 | 24.082 | 408 | Non-vegetated | 2008 | 2010 | 2 |
| 68.996 | 23.035 | 308 | Shrubs | 2008 | 2010 | 2 |
| 68.755 | 23.538 | 380 | Shrubs | 2008 | 2010 | 2 |
| 69.580 | 23.535 | 380 | Shrubs | 2008 | 2010 | 2 |
| 68.749 | 19.485 | 1713 | Non-vegetated | 2008 | 2010 | 2 |
| 69.292 | 18.133 | 1011 | Non-vegetated | 2007 | 2011 | 4 |
| 69.638 | 22.229 | 923 | Non-vegetated | 2007 | 2010 | 3 |
| 61.676 | 8.365 | 1861 | Non-vegetated | 2008 | 2010 | 2 |
| 61.684 | 8.372 | 1771 | Non-vegetated | 2008 | 2010 | 2 |
| 61.700 | 8.385 | 1559 | Non-vegetated | 2008 | 2010 | 2 |
| 61.698 | 8.401 | 1561 | Non-vegetated | 2008 | 2010 | 2 |
| 61.707 | 8.403 | 1314 | Non-vegetated | 2008 | 2010 | 2 |
| 61.701 | 8.393 | 1450 | Non-vegetated | 2008 | 2010 | 2 |
| 62.174 | 10.702 | 1630 | Non-vegetated | 2008 | 2009 | 1 |
| 62.170 | 10.703 | 1589 | Non-vegetated | 2008 | 2010 | 2 |
| 62.151 | 10.715 | 1290 | Shrubs | 2008 | 2010 | 2 |
| 61.903 | 9.275 | 1490 | Non-vegetated | 2008 | 2010 | 2 |
| 61.898 | 9.282 | 1664 | Non-vegetated | 2008 | 2010 | 2 |
| 69.291 | 18.130 | 990 | Non-vegetated | 2007 | 2009 | 2 |
| 69.249 | 20.445 | 766 | Non-vegetated | 2007 | 2009 | 2 |
| 69.642 | 22.194 | 761 | Non-vegetated | 2007 | 2010 | 3 |
| 69.681 | 22.126 | 570 | Non-vegetated | 2007 | 2010 | 3 |
| 62.149 | 9.378 | 1047 | Non-vegetated | 2005 | 2006 | 1 |
| 69.308 | 25.341 | 450 | Shrubs | 2008 | 2011 | 3 |
| 69.306 | 25.340 | 495 | Shrubs | 2008 | 2010 | 2 |
| 69.304 | 25.338 | 548 | Shrubs | 2008 | 2011 | 3 |
| 69.299 | 25.330 | 540 | Shrubs | 2008 | 2011 | 3 |
| 69.296 | 25.326 | 497 | Shrubs | 2008 | 2011 | 3 |
| 69.294 | 25.318 | 445 | Shrubs | 2008 | 2011 | 3 |
| 69.290 | 18.131 | 990 | Non-vegetated | 2007 | 2011 | 4 |
| 69.292 | 18.129 | 967 | Non-vegetated | 2007 | 2011 | 4 |
| 60.700 | 10.868 | 264 | Forest | 1994 | 2004 | 10 |
| 67.284 | 14.451 | 33 | Non-vegetated | 1994 | 2004 | 10 |

1

Table S2: Boreholes used for validation of the permafrost model. x ~~marks~~ years where data is available.

| Borehole | Lat | Lon | Elevation (m) | Depth (m) | 08/09 | 09/10 | 10/11 | 11/12 | Reference |
|---|---|---|---|---|---|---|---|---|---|
| **Abojavri BH1** | 69.642 | 22.194 | 761 | 6.6 | x | X | x | | Farbrot et al. 2013 |
| **Abojavri BH2** | 69.681 | 22.126 | 570 | 30.3 | x | X | | | Farbrot et al. 2013 |
| **BH31/PACE31** | 61.676 | 8.368 | 1894 | 20 | x | X | x | x | Isaksen et al. 2011 |
| **Guolosjavri BH1** | 69.354 | 21.211 | 786 | 32.3 | | X | x | x | Farbrot et al. 2013 |
| **Guolosjavri BH2** | 69.366 | 21.168 | 814 | 10.5 | x | | | | Farbrot et al. 2013 |
| **Guolosjavri BH3** | 69.356 | 21.061 | 780 | 10.5 | x | | | | Farbrot et al. 2013 |
| **Iskoras BH2** | 69.300 | 25.346 | 600 | 58.5 | | X | x | x | Farbrot et al. 2013 |
| **Jetta BH1** | 61.901 | 9.285 | 1560 | 19.5 | | X | x | | Farbrot et al. 2011 |
| **Jetta BH2** | 61.902 | 9.234 | 1450 | 10 | | X | x | | Farbrot et al. 2011 |
| **Jetta BH3** | 61.905 | 9.186 | 1218 | 10 | | X | x | x | Farbrot et al. 2011 |
| **Juvvass BH1** | 61.676 | 8.365 | 1861 | 10 | | X | x | x | Farbrot et al. 2011 |
| **Juvvass BH2** | 61.684 | 8.372 | 1771 | 10 | | X | x | | Farbrot et al. 2011 |
| **Juvvass BH3** | 61.697 | 8.386 | 1561 | 10 | | X | x | | Farbrot et al. 2011 |
| **Juvvass BH4** | 61.700 | 8.385 | 1559 | 10 | | X | x | x | Farbrot et al. 2011 |
| **Juvvass BH5** | 61.701 | 8.392 | 1468 | 10 | | X | x | x | Farbrot et al. 2011 |
| **Juvvass BH5** | 61.707 | 8.403 | 1314 | 10 | | X | x | x | Farbrot et al. 2011 |
| **Kistefjellet** | 69.291 | 18.130 | 990 | 24.8 | x | | | | Farbrot et al. 2013 |
| **Lavkavagge BH1** | 69.249 | 20.445 | 766 | 14 | x | X | x | x | Farbrot et al. 2013 |
| **Lavkavagge BH2** | 69.239 | 20.493 | 600 | 30.5 | x | | | | Farbrot et al. 2013 |
| **Lavkavagge BH3** | 69.224 | 20.580 | 492 | 15.8 | x | | | | Farbrot et al. 2013 |
| **Tron BH1** | 62.174 | 10.702 | 1640 | 30 | | X | x | x | Farbrot et al. 2011 |
| **Tron BH2** | 62.170 | 10.703 | 1589 | 10 | | X | x | x | Farbrot et al. 2011 |
| **Tron BH3** | 62.151 | 10.715 | 1290 | 10 | | X | x | x | Farbrot et al. 2011 |